Wireless, intraoral hybrid electronics for real-time quantification of sodium intake toward hypertension management

Yongkuk Lee[a], Connor Howe[b], Saswat Mishra[a], Dong Sup Lee[b], Musa Mahmood[a], Matthew Piper[b], Youngbin Kim[b], Katie Tieu[b], Hun-Soo Byun[c], James P. Coffey[d], Mahdis Shayan[e], Youngjae Chun[e,f], Richard M. Costanzo[g], and Woon-Hong Yeo[a,h,i,j,1]

[a]George W. Woodruff School of Mechanical Engineering, College of Engineering, Georgia Institute of Technology, Atlanta, GA 30332; [b]Department of Mechanical and Nuclear Engineering, School of Engineering, Virginia Commonwealth University, Richmond, VA 23284; [c]Department of Chemical and Biomolecular Engineering, Chonnam National University, 59626 Jeonnam, South Korea; [d]Department of Prosthodontics, School of Dentistry, Virginia Commonwealth University, Richmond, VA 23298; [e]Department of Industrial Engineering, University of Pittsburgh, Pittsburgh, PA 15261; [f]Department of Bioengineering, University of Pittsburgh, Pittsburgh, PA 15261; [g]Department of Physiology and Biophysics, School of Medicine, Virginia Commonwealth University, Richmond, VA 23298; [h]Institute for Electronics and Nanotechnology, Georgia Institute of Technology, Atlanta, GA 30332; [i]Petit Institute for Bioengineering & Bioscience, Georgia Institute of Technology, Atlanta, GA 30332; and [j]Center for Flexible Electronics, Georgia Institute of Technology, Atlanta, GA 30332

Edited by John A. Rogers, Northwestern University, Evanston, IL, and approved April 11, 2018 (received for review November 13, 2017)

Recent wearable devices offer portable monitoring of biopotentials, heart rate, or physical activity, allowing for active management of human health and wellness. Such systems can be inserted in the oral cavity for measuring food intake in regard to controlling eating behavior, directly related to diseases such as hypertension, diabetes, and obesity. However, existing devices using plastic circuit boards and rigid sensors are not ideal for oral insertion. A user-comfortable system for the oral cavity requires an ultrathin, low-profile, and soft electronic platform along with miniaturized sensors. Here, we introduce a stretchable hybrid electronic system that has an exceptionally small form factor, enabling a long-range wireless monitoring of sodium intake. Computational study of flexible mechanics and soft materials provides fundamental aspects of key design factors for a tissue-friendly configuration, incorporating a stretchable circuit and sensor. Analytical calculation and experimental study enables reliable wireless circuitry that accommodates dynamic mechanical stress. Systematic in vitro modeling characterizes the functionality of a sodium sensor in the electronics. In vivo demonstration with human subjects captures the device feasibility for real-time quantification of sodium intake, which can be used to manage hypertension.

wireless intraoral system | stretchable hybrid electronics | sodium intake quantification | hypertension management

Over the last decade, there have been rapid advances in the development of noninvasive, portable, and wearable healthcare devices (1, 2), including temperature sensors (3), glucose monitors (4), fall detectors (5), and electronic skins (6). These devices can help users achieve healthy independent living with minimal outside support. The growing demand for such devices has naturally directed attention toward the oral region, which provides great resources for disease diagnostics and health management. Electronics in the oral cavity (7, 8) can be used as biosensors, targeting specific biomarkers in saliva. Viscous saliva is a source for a noninvasive disease diagnosis since three major salivary glands diffuse multiple biomarkers (9) from blood, including DNA, RNA, protein, metabolites, and microbiota. In addition, such intraoral systems can offer monitoring of dietary intake, in regards to food-related diseases (10) such as high blood cholesterol, diabetes, and obesity. Specifically, sodium intake plays an important role in controlling blood pressure, as well as nerve and muscle function (11). Abnormal sodium levels in the body may result in severe diseases such as kidney failure (12), cardiovascular disease (13), cancer (14), and osteoporosis (15). A recent report shows that, globally, an adult consumes 3.9 g/d of sodium, which is almost twice the amount (less than 2 g/d) recommended by the World Health Organization (16). As a result, about one in three American adults suffers from hypertension (17), which leads to 7.1 million deaths, ∼13% of the total deaths worldwide, every year (18).

While advances in flexible materials and electronics have enabled various types of noninvasive health monitoring systems, they are not directly applicable for insertion in the oral cavity due to their bulky and rigid frameworks, as well as lack of biocompatibility. Miniaturized circuits with flexible sensors have been attached to a mouthguard (19) for intraoral electrochemical measurement. However, those devices are housed in a rigid plastic board, which is not capable of comfortable, direct adherence onto the oral tissue. Consequently, such devices add excessive mechanical and thermal loading and discomfort to a user, particularly considering that the oral mucosa (19, 20) is one of the most sensitive tissues in the body. Recent works (21–23) including a microfluidics-enabled wearable electronics introduced soft electronics with integrated rigid chip components on flexible membranes. These devices demonstrate wireless monitoring of signals, including EEG, ECG, temperature, and strain. However, the embedded telecommunication is restricted by bulky external receivers which lack communication capability outside a 1-m range (21), or, in some cases, less than 5 cm (22, 23).

Significance

We introduce a soft, low-profile, intraoral electronics that offers continuous real-time monitoring of sodium intake via long-range wireless telemetry. The stretchable, hybrid electronic system integrates chip-scale components and microstructured sodium sensors with stretchable interconnects, together in an ultrasoft, breathable, microporous membrane. The quantitative computational and experimental studies of antenna performance optimize the wireless electronics, offering consistent functionality with minimal loss during multimodal deformation. Examples of in vivo study with human subjects demonstrate a highly sensitive, real-time quantification of sodium intake.

Author contributions: Y.L., J.P.C., R.M.C., and W.-H.Y. designed research; Y.L., C.H., S.M., D.S.L., M.M., M.P., Y.K., K.T., J.P.C., M.S., Y.C., and W.-H.Y. performed research; Y.L., C.H., S.M., D.S.L., M.M., M.P., Y.K., K.T., H.-S.B., M.S., Y.C., R.M.C., and W.-H.Y. analyzed data; and Y.L., C.H., H.-S.B., Y.C., R.M.C., and W.-H.Y. wrote the paper.

Conflict of interest statement: R.M.C. and W.-H.Y. are inventors on Patent Application US 2017/0087363A1 that covers "Wireless implantable taste system." The other authors declare that they have no competing financial interests.

This article is a PNAS Direct Submission.

[1]To whom correspondence should be addressed. Email: whyeo@gatech.edu.

This article contains supporting information online at www.pnas.org/lookup/suppl/doi:10.1073/pnas.1719573115/-/DCSupplemental.

Published online May 7, 2018.

Here, we introduce a low-profile, hybrid electronic system with integrated circuits (ICs) and stretchable interconnects, embedded in breathable elastomeric membranes. The unobtrusive and compliant system provides a gentle, conformal integration in the oral cavity, while offering a long-range wireless, real-time quantification of sodium intake. The soft hybrid electronics with active, functional ICs overcomes the limitations of communication distance and continuous operation from passive wireless telemetry. Mechanics modeling and experimental validation demonstrates a reliable membrane circuit platform that incorporates ICs in an extremely small form factor, while accommodating multimodal bending and stretching. Antenna impedance matching and network optimization via analytical calculation and experimental study allows for stable Bluetooth connectivity between the oral cavity and an external smartphone. A microstructured, ion-selective sodium sensor with functionalized polymer membranes demonstrates a highly sensitive and selective detection of sodium ions in a food mixture. Quantitative cell viability study provides strong evidence for the device's biocompatibility. A soft microporous dental retainer shows significantly reduced thermal loading compared with typical elastomers. For easy manipulation and handling, the low-profile electronics is laminated on a dental retainer. In vivo study with human subjects demonstrates the functionality of sodium sensing by using a Bluetooth-enabled smartphone or tablet, showing real-time quantification of food intake.

Results and Discussion

Fig. 1 shows an overview of a wireless, intraoral electronic system that enables a real-time quantification of sodium intake for hypertension management. The key aspect of this system is that the hybrid electronics offers active, long-range (>10 m) wireless communication, which overcomes the limitations of near-field telemetry circuits that only allow for a few centimeters distance for communication (22, 23). The complete membranous device with ICs is incorporated onto a contoured soft dental retainer for ease of handling and noninvasive insertion into the mouth. Any Bluetooth-enabled portable device, including a personal smartphone, can easily connect with the electronics for diet management via real-time monitoring of food intake (Fig. 1*A*). The stretchable electronic device is soft, thin, and ultralight, with the membrane sodium sensor and data telemetry packages; the effective moduli, entire thickness, and total mass are 68 kPa, 2 mm, and 1.5 g, respectively (*SI Appendix*, Fig. S1).

X-ray microtomography (SkyScan 1173; Bruker) captures the small form factor of the membrane electronics, laminated on the surface of a custom-made porous retainer (Fig. 1*B*). The hybrid electronics, configured in an open-mesh, multimembrane structure, offers integration versatility with any types of bendable, foldable, and moving fixtures for body wearing or insertion. The custom-fit retainer (Fig. 1*C*), made of low-modulus, microporous elastomer [Soma Foama 15 (SF15); Smooth-On], provides great comfort when in contact with intraoral tissue. An optical image in Fig. 1*D* displays the details of the mechanically deformable electronics, enclosed by an elastomeric membrane [Ecoflex 00-30 (Eco30); Smooth-On]. The device is composed of multiple layers, including meander-patterned interconnects with ICs, dielectric membrane, and stretchable ground plane (Fig. 1*E*). For in vivo human study and clinical applications, the entire device, except the sensor detection zone (size: 2.5×2.5 mm^2 for each electrode), is completely enclosed with biocompatible elastomers (Eco30 and SF15).

The combination of newly developed transfer printing and hard–soft integration with a conventional microfabrication technique allows for successful manufacture of the novel hybrid electronics (*SI Appendix*, *Note S1* and Fig. S2). The mesh-structured ground plane, stretchable interconnects, and supporting pads for mounting of ICs (Fig. 1 *D* and *E*) are fabricated using typical microfabrication methods (24, 25). The fabricated electronic layers are separated from a carrying wafer and transferred onto a thin elastomer (Eco30, 200 μm in thickness) using material transfer printing (25, 26). The hybrid electronic system is composed of

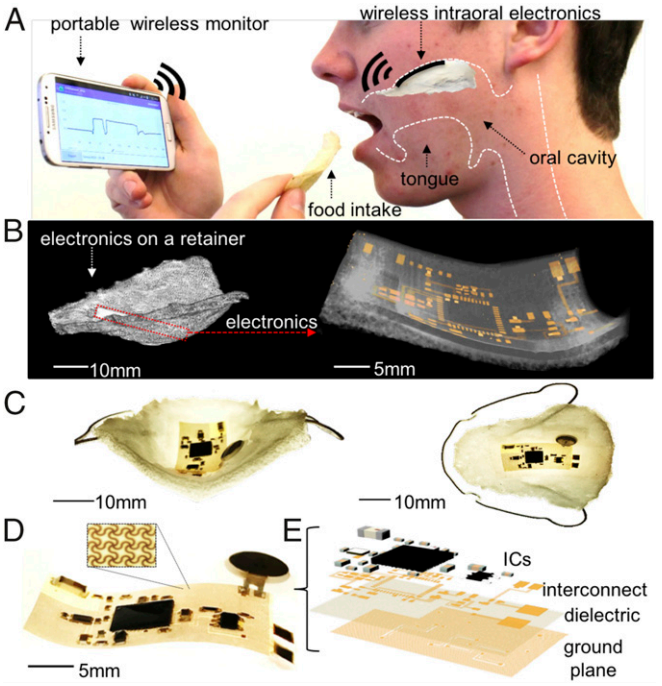

Fig. 1. System architectures and device composition. (*A*) Overview of the intraoral electronics displaying quantification of sodium intake via real-time monitoring. (*B*) X-ray micrographs of an ultrathin intraoral electronics, conformably laminated on an oral retainer (*Left*), and colorized image of circuit interconnects (*Right*) on a porous membrane. (*C*) Photos of the electronics [backside view (*Left*) and top view (*Right*)], configured in a stretchable structure with a retainer. (*D*) Zoomed-in photo of the wireless electronics. (*E*) Exploded-view illustration of the multilayer composition of the electronics in *D*, including ICs, mesh interconnects, dielectric layer, and ground plane.

multiple units: a microstructured ion-selective sodium sensor, signal filtering/amplification, Bluetooth low-energy wireless telemetry, and antenna (*SI Appendix*, Fig. S3). A miniaturized, rechargeable, microcoin battery (3.3V, 5.5 mAh, MS621FE; Seiko Instruments; see *SI Appendix*, Fig. S4) provides sustainable power to operate the intraoral device for up to 12 h of continuous measurement (*SI Appendix*, Fig. S5).

Daily uses and/or clinical applications of the intraoral system require stable, easy-to-use, long-range wireless telecommunication. We utilize a low-profile, monopole ceramic antenna that reliably provides a high frequency (~2.4 GHz), unlike dipole or microstrip antennas that require larger antenna design. A key design factor, in the use of a monopole antenna, is to incorporate an effective ground plane (27) for creation of an electrical mirror image of the antenna to maximize gain. We designed a mesh structured, Cu membrane as the ground plane (500 nm in thickness), located at the bottom layer of the electronics (Fig. 1*E*). A 1.5-μm-thick top layer consists of stretchable interconnects and contact pads (Fig. 2*A*) to integrate a microstructured sodium sensor and multiple sets of ICs (*SI Appendix*, Fig. S3). The entire area of the bottom ground plane is constructed in open-mesh, serpentine interconnects with vertical interconnect accesses (*SI Appendix*, Fig. S6). In the device configuration, a 9-μm-thick dielectric layer, made of polyimide (PI; HD MicroSystems), plays an important role as an insulator, physically protecting the ground plane during the soldering process, while offering impedance matching for the transmission line, optimizing antenna performance (*SI Appendix*, Fig. S7).

Optical microscopic images of the circuit on a soft membrane (Fig. 2*A*) show a low-power microprocessor chip, miniaturized antenna, and impedance matching network. According to the maximum power transfer theorem (28), the antenna impedance should match with the transmitter output impedance to deliver

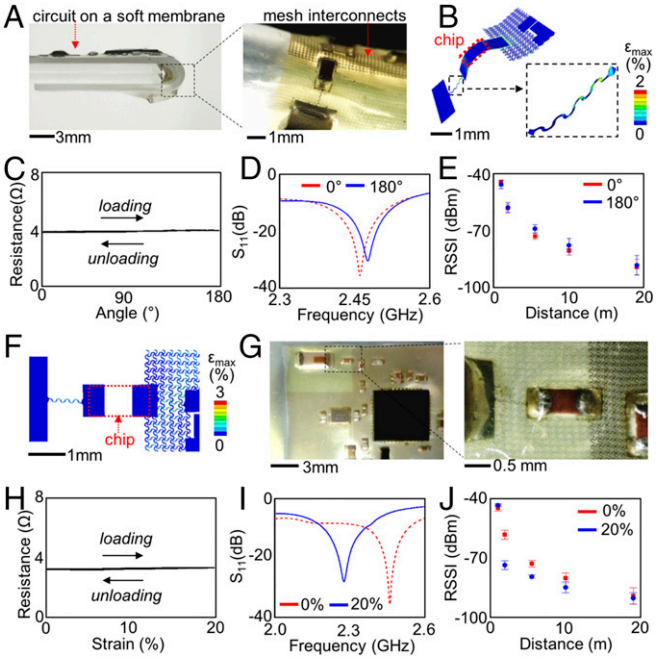

Fig. 2. Mechanical behaviors and reliability of wireless telemetry. (*A*) A device wrapped around a curved glass edge, showing the 180° bendability (radius of curvature: 1.5 mm). (*B*) FEA of the mesh structure upon 180° bending with a minimal strain (scale bar: maximum principal strain). (*C*) Electrical resistance of the device upon cyclic bending up to 180°. (*D*) Change of reflection coefficient (S11) of the antenna unit according to the frequency (gigahertz) when bending is applied from 0° to 180°. (*E*) Response of the RSSI according to the distance change. (*F*) FEA result of a stretched mesh interconnect with 20% biaxial stretching (scale bar: maximum principal strain). (*G*) Photo (*Left*) of an antenna and impedance matching network when 20% of strains are applied. The zoomed-in photo (*Right*) shows a mechanical stretching of the circuit as expected from the FEA result in *F*. (*H*) Stable electrical resistance upon cyclic stretching of the device up to 20%. (*I*) S11 response to the applied strains (20%). (*J*) RSSI response to the change of receiver distance and mechanical strain.

maximum power to the antenna. Therefore, the power loss during data transmission between the antenna and transmitter module can be minimized through the optimized impedance matching and use of a Balun filter to tune the output impedance. We optimized the circuit impedance by controlling the thickness of the dielectric layer and the width and thickness of the transmission line by following Wheeler's equation (29) (see *SI Appendix*, *Note S2* for details of the optimization process). To achieve an ideal impedance of near 50 Ω, a 9-μm-thick dielectric layer and 20-μm-wide, 1.5-μm-thick transmission line were required (*SI Appendix*, Fig. S6). In addition, the impedance matching network was tuned to operate the antenna at the frequency range between 2.4 GHz and 2.5 GHz (*SI Appendix*, Fig. S7*D*).

Fig. 2 *B*–*J* summarizes the computational and experimental results of the wireless telemetry performance under dynamic mechanical bending and biaxial strains. Computational finite element analysis (FEA; see *SI Appendix*, *Note S2* for details) estimates the maximum mechanical principal strains on the Cu metal interconnect (fracture limit: 5%) (3), focusing on antenna and transmission line, due to its mechanical isolation from the mesh ground plane. To achieve the target of 180° bending, the smallest radius of curvature is estimated as 1.5 mm for the antenna unit, which can be increased up to 4 mm for the region of the Bluetooth low-energy chip (dimension: 6 × 6 mm^2; see *SI Appendix*, Fig. S8). The circuit interconnects show negligible effect from mechanical bending up to 180°, as observed both in microscopic observation (Fig. 2*A*, *Right*) and FEA study (Fig. 2*B*). An electrical resistance measurement (Fig. 2*C*) confirms the computational result with stable resistance (maximum change: 0.12 Ω) during cyclic bending of the structure (*SI Appendix*, Fig. S9). In addition, the measurements of wireless transmission performance in Fig. 2 *D* and *E* demonstrate device functionality upon excessive bending. The reflection coefficient (S_{11}) in Fig. 2*D* indicates that the resonant frequency slightly shifted toward higher frequencies due to the mechanical deformation. The lowest S_{11} value is −30.58 dB at 2.48 GHz, which means that sufficient power (>90%) is still delivered to the antenna (30) (see *SI Appendix*, Fig. S10*A* for details of the measurement). Received signal strength (RSSI) data in Fig. 2*E* compare antenna performance between highly deformed and intact devices, which shows the consistent signal strength up to 20 m of communication distance.

Fig. 2 *F*–*J* summarizes the performance of the antenna and transmission unit under a cyclic biaxial strain. The FEA result (Fig. 2*F*) shows the mechanical stability of the mesh structure with a chip under biaxial stretching up to 20%, which is supported by microscopic observation (Fig. 2*G* and *SI Appendix*, Fig. S11). Since rigid electronic components (ICs) were directly bonded on contact islands within the mesh dielectric layer, the system represented irregular stretching, as the applied stress was not uniformly distributed. To minimize the excessive loading to the transmission line, we extended the dielectric layer to the antenna zone further while monitoring the antenna performance. The electrical resistance and antenna measurements validate the stable operation of the system upon mechanical stretching up to 20% (Fig. 2 *H*–*J*). The results show that the intraoral electronics adhered to the palate can endure the maximum tissue elongation (~10%) during phonation (31). The S_{11} measurement (Fig. 2*I*) demonstrates the resonant frequency shifted toward lower frequencies during the mechanical stretching (*SI Appendix*, Fig. S10*B*). The reflection coefficient values are changed to −7.37, −4.97, and −3.69 dB for 2.40, 2.45, and 2.50 GHz, respectively, while the lowest value is found to be −28.03 dB at around 2.28 GHz. The average reflection coefficient over the frequencies is approximately −5.15 dB, which suggests ~70% of the power is delivered to the antenna. The corresponding RSSI measurement (Fig. 2*J*) demonstrates that signal strength decreases with increased stretching, and increased distance between the communicating devices. We observed that the system was wirelessly accessible and offered continuous, consistent data transmission for distances up to 5 m, in all aforementioned tests. Overall, the quantitative mechanical and antenna studies during dynamic bending and stretching ensure the robust operation of the system in a soft oral tissue, along with the practical range of wireless communication.

A device, inserted in the oral cavity, requires a breathable, compliant material for minimized thermal and mechanical loading to the tissue. In this paper, we utilize a low-modulus microporous material, to optimize user comfort by considering the material's core properties (porosity, rigidity, and permeability). Fig. 3*A* illustrates the packaged electronics with soft, biocompatible polymers. The system consists of four layers, including the bottom-placed porous substrate (2 mm in thickness; SF15), silicone elastomeric spacer (200 μm in thickness; Eco30), circuit interconnects (1.5-mm-thick Cu), and top encapsulant (500-μm-thick Eco30). In the structure, the breathable, porous membrane (SF15) in the form of a retainer makes direct contact with the oral tissue on the palate (Fig. 1 *C* and *D* and *SI Appendix*, Fig. S12). Scanning electron microscope (SEM) images in Fig. 3*B* display a tilted and cross-sectional view of the fabricated electronics, capturing the high porosity of the tissue-contacting membrane (SF15) and stretchable mesh structure of interconnects.

We made a quantitative assessment of the membrane porosity and water vapor permeability to characterize the selected porous membrane (Fig. 3 *C* and *D*). Previous works (24, 32) have reported supreme biocompatibility of Eco30 and polydimethylsiloxane (PDMS; Dow Corning), but breathability is largely unexplored. The material's porosity is determined by measuring the weight change in immersed water (33) (*SI Appendix*, *Note S3* and Table S1). The microporous membrane (SF15) has about 30 times higher porosity

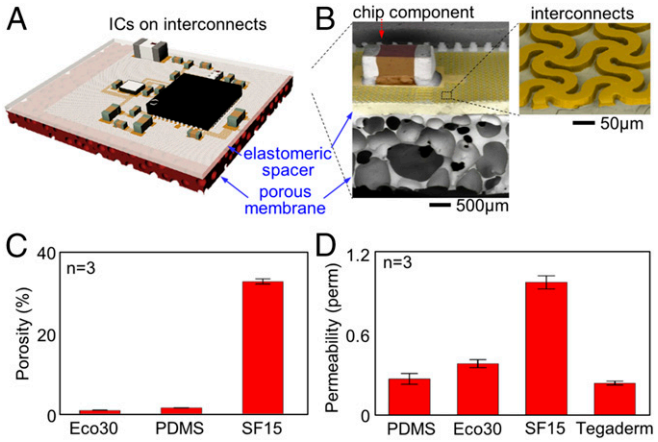

Fig. 3. Characterization of a breathable, porous material. (*A*) Illustration of a membrane integrating the fabricated electronics with ICs and stretchable interconnects. (*B*) SEM images of the cross-sectional view of the supporting substrate. (*C*) Comparison of porosity (percent) of materials including Eco30, PDMS, and SF15. (*D*) Measured permeability from four materials including PDMS, Eco30, SF15, and Tegaderm.

than typical elastomers of Eco30 and PDMS (Fig. 3*C*). The increased porosity decreases the modulus, for a softer, user-comfortable structure; SF15 has a modulus of 21 kPa, compared with Eco30 with 64 kPa and PDMS with 1.8 MPa (*SI Appendix*, Fig. S13). Measurement of water vapor transfer rate (permeability) demonstrates basic breathability of the material. The permeability is determined by the weight loss of a water container, completely sealed with testing materials, including PDMS, Eco30, SF15, and Tegaderm (Fig. 3*D* and *SI Appendix*, *Note S4* and Fig. S14). In this comparison, we added a medical-grade skin tape widely used at hospitals, Tegaderm (3M) (34), to compare the performance of breathability. The experimental result in Fig. 3*D* captures the novelty of the highly porous membrane (SF15) with much higher (at least 2.5 times) permeability than others. Note that each experiment used three different samples to determine the average and SD.

An assessment of biological comfort of materials to a tissue can include quantified thermal loading, in addition to the measured permeability. We considered the rate of heat transfer, indicating how fast the material dissipates heat from the contact tissue on the palate. A material with rapid heat transfer provides lowered thermal loading to the intraoral surface, which indicates long-term comfort. To investigate thermal properties and heat transfer of materials, we conducted computational modeling (Fig. 4 *A*–*C*) using the Bioheat Transfer Module in COMSOL Multiphysics (COMSOL Inc.; see *SI Appendix*, *Note S5* and Fig. S15). In the analysis, a device (dimension: 1.6 × 2 cm^2) with thickness of 4 mm was used. The modeled device has an initial temperature of 20 °C, making direct contact to the oral tissue (37 °C) that transfers the heat to the device. In the modeling, the device is surrounded by water to mimic the wet environment in the oral cavity. The illustration in Fig. 4*A* depicts the oral cavity model with a device adhered to the palate. This study calculates 3D temperature distribution of a material on the palate for 300 s, right after the tissue lamination. The result in Fig. 4*B* presents that the porous membrane (SF15), making the direct contact to the oral tissue, has the highest thermal dissipation, compared with others (PDMS and Eco30). The time-dynamic variation on the tissue (Fig. 4*C*) shows the heat dissipation through the material. Overall, the highly porous membrane provides lowered thermal loading to the tissue than typical elastomers.

Another important factor to consider is the biocompatibility of the device that makes direct contact with the intraoral tissue. In vitro cellular-level study demonstrates basic biocompatibility of the intraoral electronics (Fig. 4 *D*–*F*). We quantified the viability of human fibroblast cells on our device, compared with a control (polystyrene tissue culture plate; Sigma-Aldrich) based on a colorimetric assay (MTT Cell Growth Assay Kit; EMD Millipore). The result demonstrates that the number of live cells with the device is slightly lower than that with the control. However, the difference is within the statistical error range with overlapping deviations. We speculate that the contoured surface of the intraoral device, unlike the flat control, would contribute to less proliferation of cells (35).

One of the main contributions in this work is the development of a microstructured, membrane sodium sensor (Fig. 5*A*) to detect sodium intake. The ion-selective sodium electrodes (ISE) using polymers are inexpensive and easy to fabricate, while offering high selectivity, wide signal range, and rapid response time (36). The microstructured ISE includes working and reference sensors (Fig. 5 *A* and *B*), made by electroplated Pd and Ag/AgCl on a Cu membrane, respectively (*SI Appendix*, *Note S1* and Fig. S16). A waterproof, 500-μm-thick silicone elastomer (Eco30) encapsulates both electrodes, except the opening window at the center of the sensing zones. The sealed structure prevents the sodium membrane from separating from the working electrode and also protects the ISE from direct contact with solid foods during in vivo applications.

A set of in vitro experiments (Fig. 5 *C*–*E*) characterizes the selectivity, sensitivity, and long-term stability (1 wk) of the ISE for sodium detection. The time-dynamic voltage response in Fig. 5*C* shows the change of amplitudes according to the various concentrations of sodium solutions. The microfabricated ISE demonstrates a clear detection of the concentration difference as well as high sensitivity (as small as 10^{-4} M solution), which offers enough sensing spectrum for sodium detection. The sensitivity of the ISE, which is determined by the standard curve of the measured data, is 188 ± 12 mV/decade (gain = 2; see *SI Appendix*, Fig. S17 for plot). This super-Nernstian response is caused by Ag/AgCl reference electrode that acts as a Cl ion-selective electrode. With sodium bicarbonate ($NaHCO_3$; non-chloride solution), the fabricated ISE shows near-Nernstian response (120 ± 2 mV/decade; without gain, 60 ± 1 mV/decade; see *SI Appendix*, Fig. S18). Note that most sodium ions as well as chloride ions are consumed as part of salts from food, and they

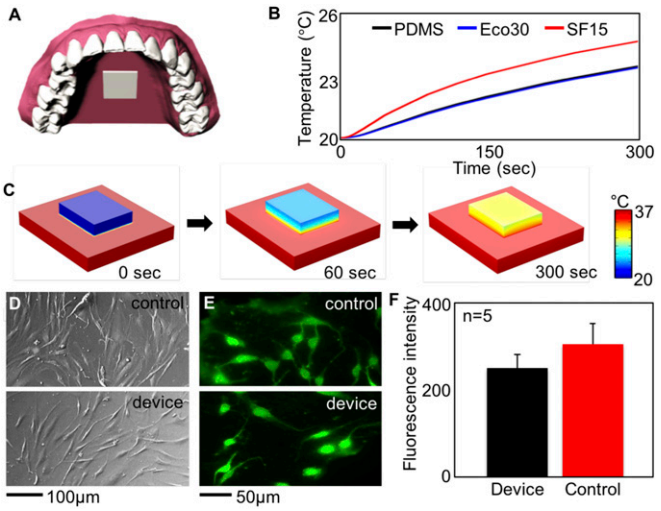

Fig. 4. Tissue compatibility and biological comfort. (*A*) Computational model for an oral cavity including the porous material. (*B*) Time-dependent temperature variation of materials on the palate in *A*. SF15 shows more enhanced heat dissipation than others. (*C*) Fast temperature distribution of SF15 when laminated on the oral tissue in *A*. (*D*) SEM images of cultured cells on a control sample (*Top*) and fabricated device (*Bottom*). (*E*) Fluorescence imaging of cultured cells on a control (*Top*) and device (*Bottom*), with green fluorescence indicating live cells. (*F*) Comparison of fluorescence intensity from live cells between the device and control.

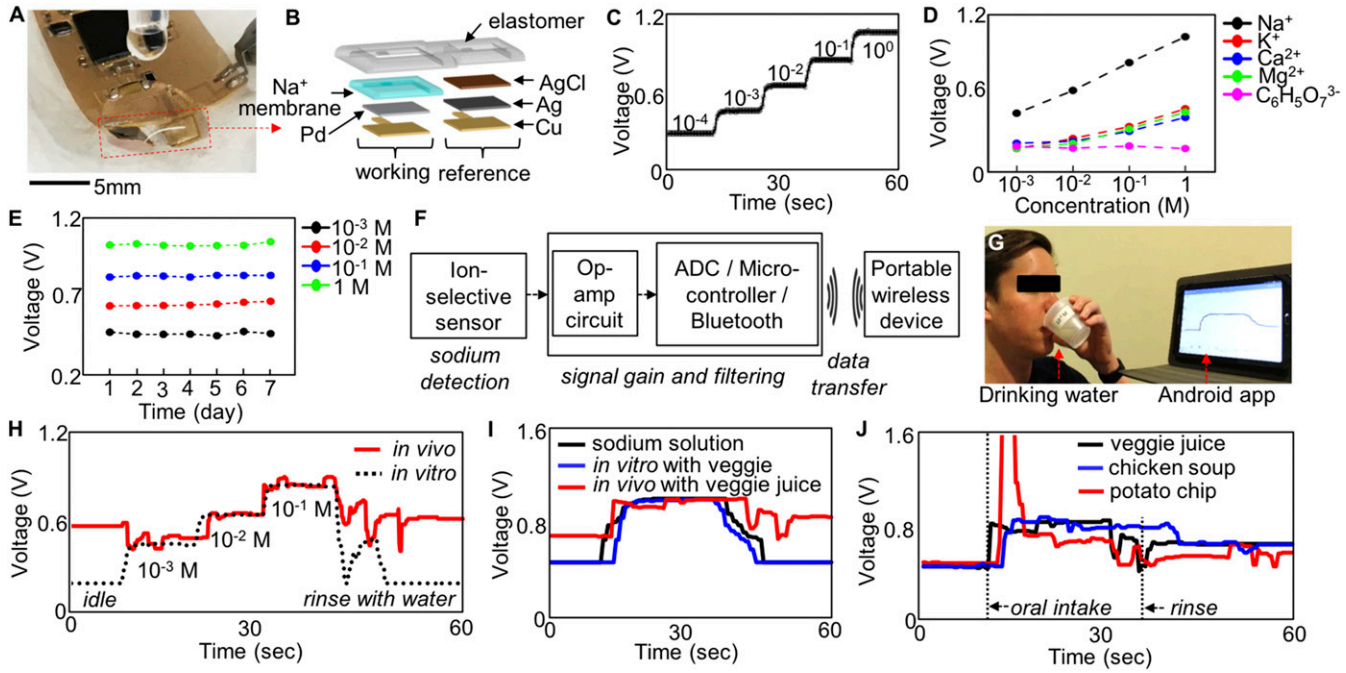

Fig. 5. Demonstration of the device functionality. (*A*) Photo of a fabricated electronic device with a microstructured sodium sensor. (*B*) Composition of multilayers for the sodium sensor featuring working and reference electrodes. (*C*) Change of voltage amplitude (volts) from the sodium sensor according to the different sodium concentrations from 1 M to 10^{-4} M. (*D*) Amplitude change of the sodium sensor according to the input solutions, including Na, K, Ca, Mg, and citric acid. (*E*) Continuous sodium detection up to 1 wk with four different sodium concentrations from 10^{-3} M to 1 M. (*F*) Flowchart showing the overall process from sodium detection to data transfer. (*G*) Photo of in vivo testing setup with a human subject and an Android application. (*H*) Comparison of in vitro and in vivo data with various sodium concentrations. (*I*) Demonstration of real-time detection of veggie juice with high sodium concentration. (*J*) In vivo, real-time measurement of different foods with a human subject.

exist at very low concentrations in food. For example, the average chloride intake is only 100 mg/d with a salt-free diet (37). Therefore, even with the presence of chloride ion interference on the Ag/AgCl electrode, its adverse effect would be negligible when it is used to detect sodium ions in food products. The ionic selectivity of the device is investigated by using five different ionic solutions, including Na^+(sodium from NaCl), K^+ (potassium from KCl), Ca^{2+} (calcium from $CaCl_2$), Mg^{2+} (magnesium from $MgCl_2$), and $C_6H_5O_7^{3-}$ (citric acid from $C_6H_8O_7$). They are commonly found in foods and drinks (38, 39). The experimental result in Fig. 5*D* demonstrates a distinctive selectivity of the fabricated sodium sensor with various concentrations of other solutions. Considering the interference from chloride ion on the Ag/AgCl electrode, the measurement data show a great selectivity of the sodium sensor. In general, K^+, Ca^{2+}, and Mg^{2+} ions with chloride exist in food with a small concentration, less than 40 mM (40), such that the selectivity of the ISE should be sufficient for specific detection of sodium intake.

In addition, a long-term stability study of the ISE (Fig. 5*E* and *SI Appendix*, Fig. S19) shows the sensor's continuous functionality for 1 wk, measured with four different sodium concentrations (10^{-3}, 10^{-2}, 10^{-1}, and 1 M). The measured average slope and its SD is 190 ± 4 mV/decade (gain = 2) for 1 wk, which indicates our sensor is stable over time, enabling continuous sodium monitoring. Overall, the in vitro study captures the ISE capability for highly specific and sensitive detection of sodium. A flowchart in Fig. 5*F* illustrates the entire process of sodium detection from the sensor to the monitoring device. The potential difference between the working and reference electrodes corresponding to sodium concentrations is loaded on the op-amp circuit with a low-pass filter. The output analog signals from the circuit are converted into digital signals with a resolution of 8 bits (~4.7 mV/resolution at the analog-to-digital converter reference voltage of 1.2 V), and they are wirelessly transmitted to an external portable device such as an Android smartphone (*SI Appendix*, Fig. S20).

We conducted a real-time recording of sodium detection with different concentrations with healthy adults (Fig. 5*G*). The intraoral system is cleaned by soap and water and a disinfectant solution (pH Neutral Disinfectant Cleaner; Australian Gold) before wearing the system in the mouth. A subject wearing the electronics sequentially drinks two sips of salty water with concentrations of 10^{-3}, 10^{-2}, and 10^{-1} M, and rinses the mouth with distilled water at the last step (see Movie S1 for details of the procedure). The same experiment in an in vitro setup (*SI Appendix*, Fig. S21) compares the recorded data with the real-time data (Fig. 5*H*). The result shows that the in vivo device offers a clear distinction of different sodium amounts, which is almost identical to the in vitro data. It should be noted that, at the idle state, the intraoral device reads 500 mV to 600 mV, since human saliva contains sodium ions with typical concentrations of 2 mM to 21 mM (41). Fig. 5*I* summarizes in vivo and in vitro sodium measurements from a veggie juice (sodium amount: 640 mg in 240 mL = 116 mM), which are compared with a pure sodium solution. Three different experiments show a similar average value (~850 mV) at high potentials. Small variations are caused by different sodium concentrations: 116, 100, and 108 mM for the sodium solution, veggie juice for in vitro, and veggie juice for in vivo, respectively. The result displays the high selectivity and sensitivity of the ISE, even with the juice that contains not only sodium but also other ingredients (potassium, protein, calcium, iron, and vitamin C). In addition, the measured data support that solid-state Ag/AgCl electrodes in the ISE have negligible interference from chloride ions during sodium detection in food. The in vivo sensor showing a higher baseline voltage from saliva in the mouth. A more comprehensive in vivo experiment in Fig. 5*J* presents sodium detection from three kinds of food with different sodium levels, including a veggie juice (640 mg in 240 mL; 116 mM), chicken noodle soup (690 mg in 242 g; 124 mM), and

potato chip (170 mg in 28 g; 264 mM). While the detected sodium from the chicken soup is 870 ± 14 mV (130 mM), close to the estimated value (124 mM), the measured value from the chip (709 ± 35 mV; 20 mM) is one order of magnitude lower than the actual amount (264 mM). We speculate that the detected sodium value from the chip is the output from the mixture with saliva, which dilutes the sodium concentration. The abrupt peak from the chip data (Fig. 5*J*) is caused by the physical contact of the solid food with the sensor. The in vitro and in vivo experiments demonstrate the feasibility of the wireless, intraoral hybrid electronics for real-time monitoring of sodium intake with high stability, sensitivity, and selectivity. Furthermore, the intraoral electronics shows the potential for estimation of the daily sodium intake along with a commercial smartphone application (e.g., MyFitnessPal in Health & Fitness) that provides brief information on sodium amounts in each food. Continuous monitoring of sodium concentration of food on a daily basis will provide eating habits of the user, which will be used to guide a better way to choose healthier food with low sodium.

The collection of materials presented here indicates that a soft, low-profile, user-comfortable electronics offers continuous real-time monitoring of sodium intake via active wireless telemetry. The stretchable hybrid system integrates chip-scale components and microstructured sodium sensors with stretchable interconnects, together in an ultrasoft, breathable membrane. The quantitative computational and experimental studies of antenna performance optimize the wireless electronics, offering consistent functionalities during multimodal deformations. Studied microporous membrane provides a great structural platform for a biocompatible interface with the tissue. Overall, this paper reports fundamental strategies to design wireless, user-comfortable, hybrid stretchable electronics for a broad range of biomedical applications (42). Future study could focus on addition of a microvolume sensor to accurately quantify daily sodium intake and further miniaturization of the electronics to house an array of multibiochemical sensors to monitor a variety of analytes in oral intake.

Materials and Methods

Details of device fabrication steps and relevant materials appear in *SI Appendix*. Also, details of theoretical analysis and computational modeling are described in *SI Appendix*. Before the human study, three volunteers (males, ages from 25 y to 40 y) were given the details of protocols, and they provided informed consent. The study was conducted at Virginia Commonwealth University (approved protocol: HM20002257) and Georgia Institute of Technology (approved protocol: H17212).

ACKNOWLEDGMENTS. W.-H.Y. acknowledges a research grant from Medarva Foundation, a seed grant from the Institute for Electronics and Nanotechnology, a grant by the Fundamental Research Program (Project PNK5061) of Korea Institute of Materials Science, and startup funding from the Woodruff School of Mechanical Engineering at Georgia Institute of Technology.

1. Rodgers MM, Pai VM, Conroy RS (2015) Recent advances in wearable sensors for health monitoring. *IEEE Sens J* 15:3119–3126.
2. Herbert R, Kim J-H, Kim YS, Lee HM, Yeo W-H (2018) Soft material-enabled, flexible hybrid electronics for medicine, healthcare, and human-machine interfaces. *Materials (Basel)* 11:E187.
3. Hattori Y, et al. (2014) Multifunctional skin-like electronics for quantitative, clinical monitoring of cutaneous wound healing. *Adv Healthc Mater* 3:1597–1607.
4. Lee H, et al. (2017) Wearable/disposable sweat-based glucose monitoring device with multistage transdermal drug delivery module. *Sci Adv* 3:e1601314.
5. Jung S, et al. (2015) Wearable fall detector using integrated sensors and energy devices. *Sci Rep* 5:17081.
6. Kim J, et al. (2014) Stretchable silicon nanoribbon electronics for skin prosthesis. *Nat Commun* 5:5747.
7. Mannoor MS, et al. (2012) Graphene-based wireless bacteria detection on tooth enamel. *Nat Commun* 3:763.
8. Kim J, et al. (2014) Non-invasive mouthguard biosensor for continuous salivary monitoring of metabolites. *Analyst (Lond)* 139:1632–1636.
9. Mishra S, et al. (2016) Recent advances in salivary cancer diagnostics enabled by biosensors and bioelectronics. *Biosens Bioelectron* 81:181–197.
10. World Health Organization (2003) *Diet, Nutrition and the Prevention of Chronic Diseases* (World Health Org, Geneva).
11. Pohl HR, Wheeler JS, Murray HE (2013) Sodium and potassium in health and disease. *Interrelations Between Essential Metal Ions and Human Diseases*, eds Sigel A, Sigel H, Sigel RKO (Springer, Dordrecht, The Netherlands), pp 29–47.
12. Perucca J, Bouby N, Valeix P, Bankir L (2007) Sex difference in urine concentration across differing ages, sodium intake, and level of kidney disease. *Am J Physiol Regul Integr Comp Physiol* 292:R700–R705.
13. Cook NR, et al. (2007) Long term effects of dietary sodium reduction on cardiovascular disease outcomes: Observational follow-up of the trials of hypertension prevention (TOHP). *BMJ* 334:885–888.
14. Tsugane S (2005) Salt, salted food intake, and risk of gastric cancer: Epidemiologic evidence. *Cancer Sci* 96:1–6.
15. Prentice A (2004) Diet, nutrition and the prevention of osteoporosis. *Public Health Nutr* 7:227–243.
16. Powles J, et al.; Global Burden of Diseases Nutrition and Chronic Diseases Expert Group (NutriCoDE) (2013) Global, regional and national sodium intakes in 1990 and 2010: A systematic analysis of 24 h urinary sodium excretion and dietary surveys worldwide. *BMJ Open* 3:e003733.
17. Nwankwo T, Yoon SS, Burt V, Gu Q (2013) Hypertension among adults in the United States: National Health and Nutrition Examination Survey, 2011-2012. *NCHS Data Brief* 1–8.
18. World Health Organization (2002) World Health Report (World Health Org, Geneva).
19. Arakawa T, et al. (2016) Mouthguard biosensor with telemetry system for monitoring of saliva glucose: A novel cavitas sensor. *Biosens Bioelectron* 84:106–111.
20. Park H, et al. (2012) A wireless magnetoresistive sensing system for an intraoral tongue-computer interface. *IEEE Trans Biomed Circuits Syst* 6:571–585.
21. Xu S, et al. (2014) Soft microfluidic assemblies of sensors, circuits, and radios for the skin. *Science* 344:70–74.
22. Lee JW, et al. (2016) Soft, thin skin-mounted power management systems and their use in wireless thermography. *Proc Natl Acad Sci USA* 113:6131–6136.
23. Kim J, et al. (2016) Battery-free, stretchable optoelectronic systems for wireless optical characterization of the skin. *Sci Adv* 2:e1600418.
24. Norton JJS, et al. (2015) Soft, curved electrode systems capable of integration on the auricle as a persistent brain-computer interface. *Proc Natl Acad Sci USA* 112: 3920–3925.
25. Lee Y, et al. (2017) Soft electronics enabled ergonomic human-computer interaction for swallowing training. *Sci Rep* 7:46697.
26. Yeo W-H, et al. (2013) Multifunctional epidermal electronics printed directly onto the skin. *Adv Mater* 25:2773–2778.
27. Pozar DM (2012) *Microwave Engineering* (Wiley, Hoboken, NJ), 4th Ed.
28. Stutzman WL, Thiele GA (2012) *Antenna Theory and Design* (Wiley, Hoboken, NJ).
29. Wheeler HA (1977) Transmission-line properties of a strip on a dielectric sheet on a plane. *IEEE Trans Microw Theory Tech* 25:631–647.
30. Shafiei MM, Moghavvemi M, Wan Mahadi WNL (2017) The parametric study and fine-tuning of bow-tie slot antenna with loaded stub. *PLoS One* 12:e0169033.
31. Birch MJ, Srodon PD (2009) Biomechanical properties of the human soft palate. *Cleft Palate Craniofac J* 46:268–274.
32. Park G, et al. (2014) Immunologic and tissue biocompatibility of flexible/stretchable electronics and optoelectronics. *Adv Healthc Mater* 3:515–525.
33. Anovitz LM, Cole DR (2015) Characterization and analysis of porosity and pore structures. *Rev Mineral Geochem* 80:61–164.
34. Roy N, et al. (2012) Significant characteristics of medical-grade polymer sheets and their efficiency in protecting hydrogel wound dressings: A soft polymeric biomaterial. *Int J Polym Mater Polym Biomater* 61:72–88.
35. Ng CKM, Yu KN (2012) Proliferation of epithelial cells on PDMS substrates with micropillars fabricated with different curvature characteristics. *Biointerphases* 7:21.
36. Cadogan A, Gao Z, Lewenstam A, Ivaska A, Diamond D (1992) All-solid-state sodium-selective electrode based on a calixarene ionophore in a poly(vinyl chloride) membrane with a polypyrrole solid contact. *Anal Chem* 64:2496–2501.
37. World Health Organization (1996) *Guidelines for Drinking-Water Quality. Vol. 2, Health Criteria and Other Supporting Information* (World Health Org, Geneva).
38. Ascherio A, et al. (1998) Intake of potassium, magnesium, calcium, and fiber and risk of stroke among US men. *Circulation* 98:1198–1204.
39. Penniston KL, Nakada SY, Holmes RP, Assimos DG (2008) Quantitative assessment of citric acid in lemon juice, lime juice, and commercially-available fruit juice products. *J Endourol* 22:567–570.
40. McGuire S (2011) U.S. Department of Agriculture and U.S. Department of Health and Human Services, Dietary Guidelines for Americans, 2010. 7th Edition, Washington, DC: U.S. Government Printing Office, January 2011. *Adv Nutr* 2:293–294.
41. Edgar WM (1992) Saliva: Its secretion, composition and functions. *Br Dent J* 172: 305–312.
42. Herbert R, et al. (2018) Soft material-enabled, flexible hybrid electronics for medicine, healthcare, and human-machine interfaces. *Materials* 11:187.